



Cite this: *Chem. Commun.*, 2018, 54, 1201

Received 20th September 2017,
Accepted 2nd January 2018

DOI: 10.1039/c7cc07342a

rsc.li/chemcomm

Ni(OH)₂–Fe₂P hybrid nanoarray for alkaline hydrogen evolution reaction with superior activity†

Xiaoping Zhang,^a Shuyun Zhu,^a Lian Xia,^a Chongdian Si,^b Fei Qu^a and Fengli Qu^{*a}

It is highly attractive to develop efficient hydrogen evolution reaction (HER) electrocatalysts under alkaline conditions. In this communication, we report the preparation of amorphous Ni(OH)₂ decorated Fe₂P nanoarray on Ti mesh (Ni(OH)₂–Fe₂P/TM) via electrodeposition. As a 3D electrode for the hydrogen evolution reaction, such Ni(OH)₂–Fe₂P/TM demonstrates superior catalytic activity. Moreover, the as-prepared electrocatalyst requires an overpotential of only 76 mV to drive a current density of 10 mA cm⁻², which is 94 mV less than that for Fe₂P/TM. It also shows strong long-term electrochemical durability with its catalytic activity being maintained for at least 20 h.

The depletion of fossil fuels and severe environmental pollution concerns have caused an urgent demand for clean and sustainable alternative energy sources.^{1,2} Hydrogen is a clean and renewable energy carrier and has been widely considered as a promising alternative to fossil fuels owing to its high energy density and no byproduct-formation upon combustion.^{3–7} Electrochemical water splitting offers a facile pathway to produce pure hydrogen. Currently, Pt is regarded as the most active catalyst for the hydrogen evolution reaction (HER), but suffers from low abundance and high cost, hindering its large-scale application.^{8,9} Thus, it is highly desired to develop low-cost and high-efficiency alkaline HER catalysts.¹⁰

Transition metal phosphides (TMPs), such as Ni₂P,^{11–14} CoP,^{15,16} and Cu₃P,^{17–19} have been widely employed as electrocatalysts for the HER. Compared with the above mentioned catalysts, Fe₂P also exhibits high HER activity in acidic solutions,²⁰ but its activity in alkaline media is limited owing to the sluggish kinetics of the water dissociation process.²¹ Hence, promoting the water dissociation of Fe₂P in alkaline

media is key to improving the electrocatalytic hydrogen production. Recently, several reports have demonstrated that the combination of Ni(OH)₂ with other catalysts could significantly enhance the HER activity in alkaline media,^{22,23} in which the edges of Ni(OH)₂ promote the dissociation of water and concomitant generation of hydrogen intermediates (H_{ad}) that subsequently adsorb on catalyst surfaces and finally recombine into molecular hydrogen.^{23,24} Based on this strategy, it is highly desired to develop Ni(OH)₂ and Fe₂P hybrid toward achieving high activity for the alkaline HER.

In this communication, we report the combination of amorphous Ni(OH)₂ with Fe₂P nanoarray hybrid supported on Ti mesh (Ni(OH)₂–Fe₂P/TM) via electrodeposition for efficient hydrogen evolution. As a hydrogen-evolving catalyst electrode, the Ni(OH)₂–Fe₂P/TM shows superior activity in 1.0 M KOH, requiring an overpotential of only 76 mV to drive a geometrical current density of 10 mA cm⁻², which is 94 mV less than that for Fe₂P/TM. It also demonstrates strong long-term durability with its catalytic activity being maintained for at least 20 h.

Fig. 1a shows the X-ray diffraction (XRD) patterns of Fe₂P/TM and Ni(OH)₂–Fe₂P/TM. As observed, the peaks of Fe₂P/TM at 35.3°, 40.3°, 44.2°, 52.9°, and 63.3° are indexed to the (200), (111), (201), (002), and (220) planes of Fe₂P (JCPDS No. 65-1990), respectively. Other peaks are typical diffraction peaks of the Ti mesh (JCPDS No. 44-1294). After Ni(OH)₂ deposition, the intensity of the Fe₂P-related diffraction characteristic peaks decreases and no peaks of Ni(OH)₂ are detected, confirming the formation of amorphous Ni(OH)₂ on the surface of Fe₂P. The scanning electron microscopy (SEM) image of Fe₂P/TM (Fig. 1b) indicates that the surface of TM is coated with Fe₂P nanoarrays. As shown in Fig. 1c, the SEM image suggests that Ni(OH)₂–Fe₂P/TM still preserves its initial morphology after Ni(OH)₂ deposition. The transmission electron microscopy (TEM) images (Fig. 1d and f) demonstrate that Fe₂P and Ni(OH)₂–Fe₂P have a typical nanoarray structure. The high-resolution transmission electron microscopy (HRTEM) image taken from Fe₂P (Fig. 1e) reveals well-resolved lattice fringes with an interplanar distance of 0.224 nm corresponding to the (111) plane of Fe₂P, consistent with the XRD result.

^a College of Chemistry and Chemical Engineering, Qufu Normal University, Qufu 273165, Shandong, China. E-mail: fengliquhn@hotmail.com

^b Shandong Engineering Research Center of Chemical Intermediate, Jining University, Qufu 273155, China

† Electronic supplementary information (ESI) available: Experimental section and supplementary figures. See DOI: 10.1039/c7cc07342a

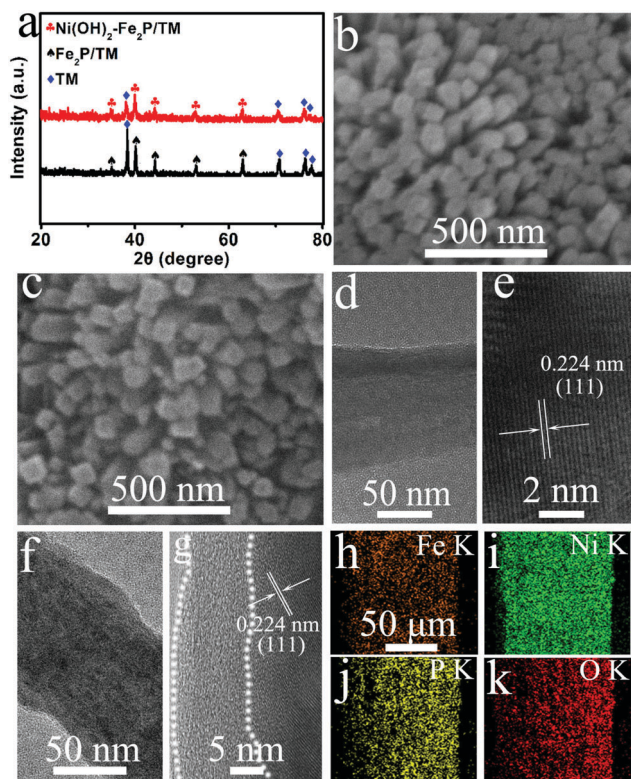


Fig. 1 (a) XRD patterns for $\text{Fe}_2\text{P}/\text{TM}$ and $\text{Ni}(\text{OH})_2\text{-Fe}_2\text{P}/\text{TM}$. SEM images of (b) $\text{Fe}_2\text{P}/\text{TM}$ and (c) $\text{Ni}(\text{OH})_2\text{-Fe}_2\text{P}/\text{TM}$. TEM and HRTEM images of (d and e) Fe_2P and (f and g) $\text{Ni}(\text{OH})_2\text{-Fe}_2\text{P}$. (h–k) EDX elemental mapping images of $\text{Ni}(\text{OH})_2\text{-Fe}_2\text{P}/\text{TM}$.

For $\text{Ni}(\text{OH})_2\text{-Fe}_2\text{P}$, the HRTEM image confirms a thin layer of amorphous $\text{Ni}(\text{OH})_2$ deposited on Fe_2P (Fig. 1g). The energy-dispersive X-ray (EDX) spectrum (Fig. S1, ESI[†]) for $\text{Ni}(\text{OH})_2\text{-Fe}_2\text{P}/\text{TM}$ confirms the existence of Fe, Ni, P, and O elements in the product; the EDX elemental mapping images (Fig. 1h–k) further suggest the uniform distribution of Fe, Ni, P, and O elements in $\text{Ni}(\text{OH})_2\text{-Fe}_2\text{P}/\text{TM}$.

Fig. 2 presents the X-ray photoelectron spectroscopy (XPS) spectrum of $\text{Ni}(\text{OH})_2\text{-Fe}_2\text{P}$, indicating the presence of the elements Fe, Ni, P, and O. In Fig. 2a, the peaks at 708.2 and 721.0 eV corresponding to $\text{Fe } 2p_{3/2}$ and $\text{Fe } 2p_{1/2}$, respectively, illustrate the formation of Fe^{2+} .²⁵ Moreover, the binding energies (BEs) at 711.2 and 724.0 eV with two shakeup satellite peaks (identified as “Sat.”) also correspond to Fe^{2+} . In the Ni 2p XPS spectrum (Fig. 2b), two major peaks with BEs of 856.5 and 874.1 eV are observed, corresponding to $\text{Ni } 2p_{3/2}$ and $\text{Ni } 2p_{1/2}$,^{26,27} respectively. The spin-orbit splitting energy between the two Ni 2p peaks is 17.7 eV, indicating the presence of the $\text{Ni}(\text{OH})_2$ phase.²⁷ In addition, the BEs at 862.0 and 880.4 eV with two shakeup satellites peaks also correspond to Ni^{2+} . Fig. 2c shows the XPS spectrum in the P 2p region. Two peaks at 130.0 and 128.8 eV are ascribed to $\text{P } 2p_{1/2}$ and $\text{P } 2p_{3/2}$, respectively.^{28,29} The peak at 133.0 eV can be assigned to the P–O species arising from superficial oxidation of P. The spectrum for the O 1s region (Fig. 2d) shows two oxygen contributions. The peak at 531.2 eV is usually associated with oxygen in the OH^- groups.^{27,30,31}

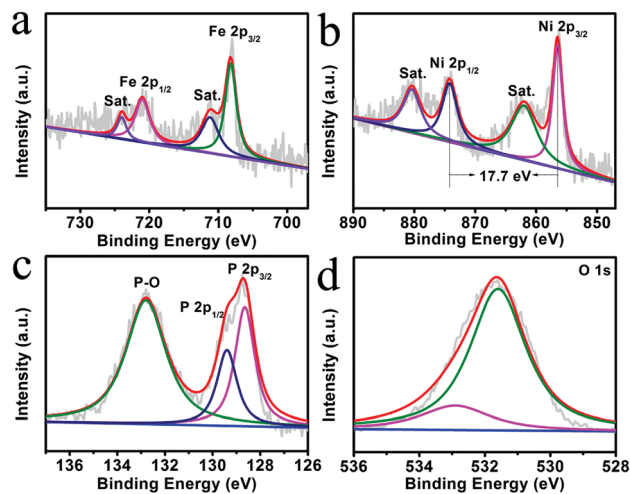


Fig. 2 XPS spectra of $\text{Ni}(\text{OH})_2\text{-Fe}_2\text{P}$ in the (a) Fe 2p, (b) Ni 2p, (c) P 2p, and (d) O 1s regions.

Furthermore, the peak at 532.9 eV can be attributed to the multiplicity of physi- and chemisorbed water on the surface.^{27,32}

To investigate the HER performance, the $\text{Ni}(\text{OH})_2\text{-Fe}_2\text{P}/\text{TM}$ (loading: 1.34 mg cm^{-2}) was tested by linear sweep voltammetry (LSV) in 1.0 M KOH with a scan rate of 5 mV s^{-1} . For comparison, $\text{Fe}_2\text{P}/\text{TM}$, Pt/C on TM (Pt/C loading: 1.34 mg cm^{-2}), and bare TM were tested in the 1.0 M KOH. On account of the direct reflection of the intrinsic behavior of catalysts, the iR correction was employed to eliminate the effect of ohmic resistance of all the original data unless it is a special case.^{33–35} Fig. 3a shows the LSV curves on the reversible hydrogen electrode (RHE) scale. It compares the HER performance of bare TM, $\text{Fe}_2\text{P}/\text{TM}$, $\text{Ni}(\text{OH})_2\text{-Fe}_2\text{P}/\text{TM}$ and Pt/C coated on TM. It is observed that Pt/C exhibits outstanding HER catalytic activity, while the bare TM exhibits much poorer HER activity within the examined potential window.

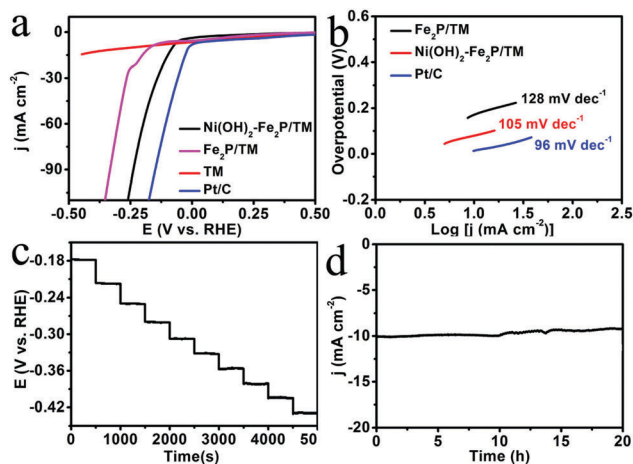


Fig. 3 (a) LSV curves of Pt/C, $\text{Ni}(\text{OH})_2\text{-Fe}_2\text{P}/\text{TM}$, $\text{Fe}_2\text{P}/\text{TM}$ and bare TM for HER. (b) Tafel plots for Pt/C, $\text{Ni}(\text{OH})_2\text{-Fe}_2\text{P}/\text{TM}$ and $\text{Fe}_2\text{P}/\text{TM}$. (c) Multi-current process of $\text{Ni}(\text{OH})_2\text{-Fe}_2\text{P}/\text{TM}$. The current density started at 40 mA cm^{-2} and ended at 220 mA cm^{-2} , with an increment of 20 mA cm^{-2} per 500 s without iR correction. (d) Time-dependent current density curves for $\text{Ni}(\text{OH})_2\text{-Fe}_2\text{P}/\text{TM}$. All experiments were carried out in 1.0 M KOH.

Impressively, Ni(OH)₂-Fe₂P/TM demands an overpotential of only 76 mV to drive a geometrical catalytic current density of 10 mA cm⁻², which is 94 mV less than that for Fe₂P/TM ($\eta_{10\text{ mA cm}^{-2}} = 170\text{ mV}$) owing to the fact that the edges of Ni(OH)₂ promote the dissociation of water and concomitantly generate hydrogen intermediates (H_{ad}) that are then adsorbed on the nearby Fe₂P and subsequently recombined to form H₂.²³ Therefore, the combination of Ni(OH)₂ and Fe₂P can enhance the HER performance. Moreover, as shown in Fig. S2 (ESI[†]), we further measured the LSV curves of Ni(OH)₂-Fe₂P/TM under 0.1 and 0.5 M KOH. The catalyst requires overpotentials of 285 and 196 mV to drive 10 mA cm⁻² in 0.1 and 0.5 M KOH, respectively. A more detailed comparison is listed in Table S1 (ESI[†]). The Tafel plots are fitted with the equation $\eta = b \log j + a$ (where j is the current density and b is the Tafel slope). As shown in Fig. 3b, the Tafel slopes are 96, 105 and 128 mV dec⁻¹ for Pt/C, Ni(OH)₂-Fe₂P/TM and Fe₂P/TM, respectively, indicating the good kinetics of Ni(OH)₂-Fe₂P/TM. The mechanism of the HER in alkaline media is typically treated as a combination of three elementary steps: the Volmer step-water dissociation and formation of a reactive intermediate H_{ad} ($2\text{H}_2\text{O} + \text{M} + 2\text{e}^- \rightleftharpoons 2\text{M}-\text{H}_{\text{ad}} + 2\text{OH}^-$), followed by either the Heyrovsky step ($\text{H}_2\text{O} + \text{H}_{\text{ad}} + \text{M} + \text{e}^- \rightleftharpoons \text{M} + \text{H}_2 + \text{OH}^-$) or the Tafel recombination step ($2\text{M}-\text{H}_{\text{ad}} \rightleftharpoons 2\text{M} + \text{H}_2$). Based on the kinetic models of HER, Tafel slopes of 120, 40, or 30 mV dec⁻¹ will be achieved if the Volmer, Heyrovsky, or Tafel step is the rate-determining step, respectively. The Tafel slopes for Fe₂P/TM and Ni(OH)₂-Fe₂P/TM are 128 and 105 mV dec⁻¹, respectively, suggesting that the HER proceeds on both catalysts through the Volmer–Heyrovsky mechanism. Moreover, the Volmer step of HER on Ni(OH)₂-Fe₂P/TM is clearly accelerated as Ni(OH)₂ promotes the dissociation of water in alkaline media.^{23,36} Fig. 3c shows a multi-current step chrono-potentiometric curve for Ni(OH)₂-Fe₂P/TM in 1.0 M KOH with the current density increasing from 40 to 220 mA cm⁻² (20 mA cm⁻² per 500 s). The potential immediately levels off at -0.18 V at the start-current value and remains unchanged for the remaining 500 s. The other steps exhibit similar results, indicating the excellent conductivity, mechanical robustness and mass transport of the Ni(OH)₂-Fe₂P/TM electrode.^{37,38} The stability is a significant parameter for evaluating the practicability of electrocatalysts. We investigated LSV curves of Ni(OH)₂-Fe₂P/TM before and after 500 cyclic voltammetry (CV) cycles as shown in Fig. S3 (ESI[†]). As observed, this electrode shows negligible current loss after 500 CV cycles in 1.0 M KOH, indicating the high stability of Ni(OH)₂-Fe₂P/TM. Furthermore, Fig. 3d shows the time-dependent current density curve at a fixed overpotential of 76 mV; the current density shows negligible loss after 20 h of electrolysis. The XRD pattern is shown in Fig. S4 (ESI[†]); the diffraction peaks after stability test are consistent with the Ni(OH)₂-Fe₂P/TM before the stability test. The XPS spectra of Ni(OH)₂-Fe₂P/TM show no change in the peaks before and after the stability test (Fig. S5, ESI[†]). As shown in Fig. S6 (ESI[†]), the SEM image shows that the morphology of the catalyst has a small change after the stability test, leading to a slight decrease. The morphology of Ni(OH)₂-Fe₂P/TM after the stability test still preserves the nanoarray feature. These results suggest the high durability of Ni(OH)₂-Fe₂P/TM in alkaline media.

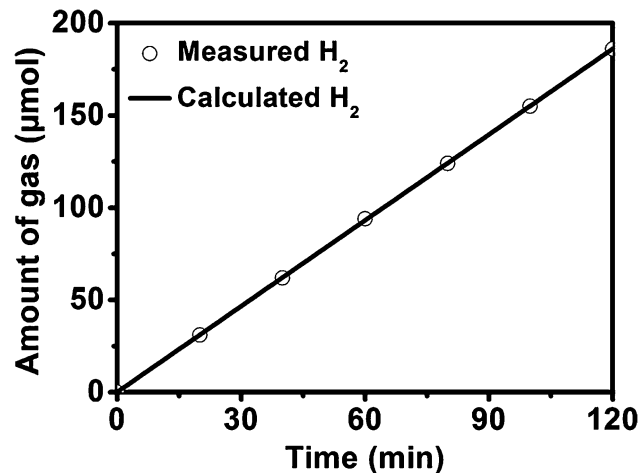


Fig. 4 The amount of gas theoretically calculated and experimentally measured versus time for hydrogen evolution of Ni(OH)₂-Fe₂P/TM.

The Faradaic efficiency (FE) and electrochemical surface area also have a significant effect on HER performance. The FE of Ni(OH)₂-Fe₂P/TM was measured by gas chromatography analysis and quantified with a calibrated pressure sensor of a H-type electrolytic cell.³⁹ The plot in Fig. 4 shows that the amount of H₂ produced increased with the electrolysis process in 1.0 M KOH. The FE of the HER process is calculated to be nearly 100%. The electrochemical double layer capacitances (C_{dl}) of the catalyst were determined to calculate the electrochemical surface area.^{40–42} Fig. S7 (ESI[†]) shows the cyclic voltammograms (CVs) of Fe₂P/TM and Ni(OH)₂-Fe₂P/TM at scan rates of 20, 60, 100, 140, 180, 220, 260, and 300 mV s⁻¹. It is clear that the C_{dl} of Ni(OH)₂-Fe₂P/TM (3.54 mF cm⁻²) is higher than that of Fe₂P/TM (0.65 mF cm⁻²), suggesting the much higher surface roughness of Ni(OH)₂-Fe₂P/TM. We can conclude that the rough nanoarray structure with high surface area makes a great contribution to the high HER catalytic activity of Ni(OH)₂-Fe₂P/TM.

In summary, Ni(OH)₂-Fe₂P/TM was successfully developed *via* electrodeposition of Ni(OH)₂ on Fe₂P/TM nanoarray. As a 3D catalyst electrode for efficient hydrogen evolution reaction, such Ni(OH)₂-Fe₂P/TM drives 10 mA cm⁻² at an overpotential of only 76 mV in 1.0 M KOH. It also demonstrates the strong long-term electrochemical durability with its catalytic activity being maintained for at least 20 h. This study not only provides us an attractive earth-abundant catalyst material for electrolytic hydrogen production in alkaline media, but would also open up an exciting new avenue to the rational design and fabrication of transition metal hydroxide–metal phosphides for hydrogen evolution reaction and other applications.

This work was supported by the National Natural Science Foundation of China (No. 21775089, 21375076, 21405094, 21505084, 21405093), the Natural Science Foundation Projects of Shandong Province (No. ZR2017JL010, ZR2017QB008, ZR2017LEE006), the China postdoctoral science foundation funded project (2017M610406), and the key research and development plan of Jining city.

Conflicts of interest

There are no conflicts of interest to declare.

References

- 1 A. J. Bard and M. A. Fox, *Acc. Chem. Res.*, 1995, **28**, 141–145.
- 2 J. Chow, R. J. Kopp and P. R. Portney, *Science*, 2003, **302**, 1528–1531.
- 3 M. S. Dresselhaus and I. L. Thomas, *Nature*, 2001, **414**, 332–337.
- 4 J. A. Turner, *Science*, 2004, **305**, 972–974.
- 5 R. F. Service, *Science*, 2009, **324**, 1257–1259.
- 6 L. Li, J. G. Bell, S. Tang, X. Lv, C. Wang, Y. Xing, X. Zhao and K. M. Thomas, *Chem. Mater.*, 2014, **26**, 4679–4695.
- 7 X. Wang, Y. V. Kolen'ko, X. Bao, K. Kovnir and L. Liu, *Angew. Chem., Int. Ed.*, 2015, **54**, 8188–8192.
- 8 J. Greeley, J. K. Norskov, L. A. Kibler, A. M. El-Aziz and D. M. Kolb, *ChemPhysChem*, 2006, **7**, 1032–1035.
- 9 W. Sheng, H. A. Gasteiger and Y. Shao-Horn, *J. Electrochem. Soc.*, 2010, **157**, B1529–B1536.
- 10 Z. Xing, X. Yang, A. M. Asiri and X. Sun, *ACS Appl. Mater. Interfaces*, 2016, **8**, 14521–14526.
- 11 B. You, N. Jiang, M. Sheng, M. W. Bhushan and Y. Sun, *ACS Catal.*, 2016, **6**, 714–721.
- 12 Z. Pu, Q. Liu, C. Tang, A. M. Asiri and X. Sun, *Nanoscale*, 2014, **6**, 11031–11034.
- 13 E. J. Popczun, J. R. McKone, C. G. Read, A. J. Biacchi, A. M. Wiltrout, N. S. Lewis and R. E. Schaak, *J. Am. Chem. Soc.*, 2013, **135**, 9267–9270.
- 14 X. Wang, Y. V. Kolen'ko and L. Liu, *Chem. Commun.*, 2015, **51**, 6738–6741.
- 15 K. Xu, H. Ding, M. Zhang, M. Chen, Z. Hao, L. Zhang, C. Wu and Y. Xie, *Adv. Mater.*, 2017, **29**, 1606980.
- 16 J. Tian, Q. Liu, A. M. Asiri and X. Sun, *J. Am. Chem. Soc.*, 2014, **136**, 7587–7590.
- 17 A. Han, H. Zhang, R. Yuan, H. Ji and P. Du, *ACS Appl. Mater. Interfaces*, 2017, **9**, 2240–2248.
- 18 S. Wei, K. Qi, Z. Jin, J. Cao, W. Zheng, H. Chen and X. Cui, *ACS Omega*, 2016, **1**, 1367–1373.
- 19 J. Tian, Q. Liu, N. Cheng, A. M. Asiri and X. Sun, *Angew. Chem., Int. Ed.*, 2014, **53**, 9577–9581.
- 20 Z. Huang, C. Lv, Z. Chen, Z. Chen, F. Tian and C. Zhang, *Nano Energy*, 2015, **12**, 666–674.
- 21 D. Strmcnik, M. Uchimura, C. Wang, R. Subbaraman, N. Danilovic, D. Vliet, A. P. Paulikas, V. R. Stamenkovic and N. M. Markovic, *Nat. Chem.*, 2013, **5**, 300–306.
- 22 B. Zhang, J. Liu, J. Wang, Y. Ruan, X. Ji, K. Xu, C. Chen, H. Wan, L. Miao and J. Jiang, *Nano Energy*, 2017, **37**, 74–80.
- 23 R. Subbaraman, D. Tripkovic, D. Strmcnik, K.-C. Chang, M. Uchimura, A. P. Paulikas, V. R. Stamenkovic and N. M. Markovic, *Science*, 2011, **334**, 1256–1260.
- 24 R. Kaviani, S. Choi, J. Park, T. Liu, H. C. Peng, N. Lu, J. Wang, M. J. Kim, Y. Xia and S. W. Lee, *J. Mater. Chem. A*, 2016, **4**, 12392–12397.
- 25 X. Ren, W. Wang, R. Ge, S. Hao, F. Qu, G. Du, A. M. Asiri, Q. Wei, L. Chen and X. Sun, *Chem. Commun.*, 2017, **53**, 9000–9003.
- 26 J. W. Lee, T. Ahn, D. Soundararajan, J. M. Koc and J. Kim, *Chem. Commun.*, 2011, **47**, 6305–6307.
- 27 Y. Su, K. Xiao, N. Li, Z. Liu and S. Qiao, *J. Mater. Chem. A*, 2014, **2**, 13845–13853.
- 28 P. Jiang, Q. Liu, Y. Liang, J. Tian, A. M. Asiri and X. Sun, *Angew. Chem., Int. Ed.*, 2014, **53**, 12855–12859.
- 29 W. Li, D. Xiong, X. Gao, W. G. Song, F. Xia and L. Liu, *Catal. Today*, 2017, **287**, 122–129.
- 30 B. P. Payne, M. C. Biesinger and N. S. McIntyrea, *J. Electron Spectrosc. Relat. Phenom.*, 2012, **185**, 159–166.
- 31 C. Zhao, X. Wang, S. Wang, Y. Wang, Y. Zhao and W. Zheng, *Int. J. Hydrogen Energy*, 2012, **37**, 11846–11852.
- 32 Z. Liu, Q. Xu, J. Wang, N. Li, S. Guo, Y. Su, H. Wang, J. Zhang and S. Chen, *Int. J. Hydrogen Energy*, 2013, **38**, 6657–6662.
- 33 C. Tang, A. M. Asiri and X. Sun, *Chem. Commun.*, 2016, **52**, 4529–4532.
- 34 Z. Xing, Q. Liu, A. M. Asiri and X. Sun, *Adv. Mater.*, 2014, **26**, 5702–5707.
- 35 R. Zhang, C. Tang, R. Kong, G. Du, A. M. Asiri, L. Chen and X. Sun, *Nanoscale*, 2017, **9**, 4793–4800.
- 36 Z. Xing, D. Wang, Q. Li, A. M. Asiri and X. Sun, *Electrochim. Acta*, 2016, **210**, 729–733.
- 37 C. Tang, N. Cheng, Z. Pu, W. Xing and X. Sun, *Angew. Chem., Int. Ed.*, 2015, **54**, 9351–9355.
- 38 X. Lu and C. Zhao, *Nat. Commun.*, 2015, **6**, 6616.
- 39 X. Ren, R. Ge, Y. Zhang, D. Liu, D. Wu, X. Sun, B. Du and Q. Wei, *J. Mater. Chem. A*, 2017, **5**, 7291–7294.
- 40 C. C. L. McCrory, S. Jung, J. C. Peters and T. F. Jaramillo, *J. Am. Chem. Soc.*, 2013, **135**, 16977–16987.
- 41 H. Du, X. Zhang, Q. Tan, R. Kong and F. Qu, *Chem. Commun.*, 2017, **53**, 12012–12015.
- 42 X. Zhang, C. Si, X. Guo, R. Kong and F. Qu, *J. Mater. Chem. A*, 2017, **5**, 17211–17215.